International Journal of Heat and Fluid Flow 29 (2008) 1211–1220

Contents lists available at ScienceDirect

International Journal of Heat and Fluid Flow

journal homepage: www.elsevier.com/locate/ijhff

Micro-PIV and CFD characterization of flows in a microchannel: Velocity profiles, surface roughness and Poiseuille numbers

Gonçalo Silva, Nuno Leal, Viriato Semiao *

Mechanical Engineering Department, Instituto Superior Tecnico, Universidade Tecnica de Lisboa, Avenida Rovisco Pais, 1049-001 Lisbon, Portugal

ARTICLE INFO

Article history:
Received 22 November 2007
Received in revised form 22 February 2008
Accepted 18 March 2008
Available online 15 May 2008

Keywords:
Micro-PIV
Microfluidics
CFD
Friction factor
Poiseuille number
Wall roughness

ABSTRACT

Microfluidics is a promising technology, although the governing physical mechanisms are still not quite understood due to the difficulties arising in measuring at such small scales. This work intends to bring some insight on the influence of surface phenomena in microscale flows by proposing a different method to quantify such influence. In this new method, detailed velocity measurements are performed to evaluate the influence on the flow of the surface phenomena instead of using measured bulk flow properties. For that micro-Particle Image Velocimetry (micro-PIV) is used to characterize the flow kinematics inside a DantecDynamics® microchannel (with hydraulic diameter of 637 μm) that possesses rather rough walls (relative roughness of 1.6%) and a very irregular cross-section shape. Two-dimensional velocity profiles were measured in 61 horizontal planes to define the three-dimensional laminar flows ($Re \leqslant 50$). Integration of the velocity profiles yielded volumetric flow rates with a maximum deviation of 3% from the measured volume of fluid discharged as function of time, which gives the magnitude of the bias error of the experimental technique. Effects of walls roughness were quantified by comparing Poiseuille numbers obtained from experimental velocity profiles against those obtained from CFD predictions for the same operating conditions but with hydrodynamically smooth walls, according to the new method proposed herein. Those Poiseuille numbers differed 11% demonstrating the need to account for wall roughness in microflows.

1. Introduction

In the last few decades microfluidics have gained increasing interest within the scientific community. Several researchers devoted growing efforts to improve understanding of physical phenomena occurring in flows at small length-scale geometries, with characteristic lengths ranging from 1 to 1000 μm, and to develop their technological applications. Bayraktar and Pidugu (2006) established velocities below 100 cm/s as those characteristic of fluid flows at such scales and defined the driving forces as pressure gradients, applied electrical fields (electrophoresis and electroosmosis), capillary forces and free surface phenomena, like gradients in the interfacial tension as in Marangoni flows.

Microfluidics-based technologies are attractive because of their high potential to increase considerably surface transport mechanisms of momentum, energy and mass, due to their inherent greater surface/volume ratio. These surface mechanisms may even become dominant due to the amplification of the surface-based effects on transport phenomena at length-scales below 1000 μm, as first stated by Went (1968) in his pioneer work. This last feature may require adjustments of the conventional macroscale Fluid Mechanics theory to be applied to microfluidics as it neglects those surface phenomena, as mentioned by Gad-el-Hak (1999), Hetsroni et al. (2005) and Magueijo et al. (2006). Such phenomena are the surface tension effects caused by the different fluid/wall interfacial affinity at hydrophilic or hydrophobic channels walls; the presence of bubbles; the wall roughness that, in cases of high relative values, may play a crucial role as it changes the velocity profiles due to a change of momentum transfer; and the existence of high shear rates and stress rates capable of promoting a non-Newtonian behaviour of commonly Newtonian fluids. Even though, several works report similar experiments on microfluidic flows with different results and are explained by the authors through different approaches. This denotes the ill-understood mechanisms that occur in such microscale flows. Many researchers carried out numerous studies determining the pressure drop/friction factor, i.e. the Poiseuille constant *fRe* quantification, to ascertain the existence of possible microfluidic deviations to the macroscale theory, basing their studies on the assumption of constant *fRe* values for a steady, laminar, incompressible, fully developed and pressure-driven flow with constant thermodynamic properties within constant cross-sectional channels.

Analyses of results are, however, diverse. On one side, there are authors stating that the Navier–Stokes equations traditionally applied to macroscale flows must be adapted in order to account

* Corresponding author. Tel.: +351 218417726; fax: +351 218475545.
E-mail address: ViriatoSemiao@ist.utl.pt (V. Semiao).

0142-727X/$ - see front matter © 2008 Elsevier Inc. All rights reserved.
doi:10.1016/j.ijheatfluidflow.2008.03.013

Nomenclature

D_h	microchannel hydraulic diameter [m]	x	streamwise direction (length) [m]
f	friction factor	y	crosswise direction (width) [m]
p	static pressure [Pa]	z	crosswise direction (height) [m]
PIV	particle image velocimetry	ΔQ_v	volumetric flow rate error
Q	volumetric flow rate [m^3/s]	ΔQ_m	momentum flow rate error
Q_v	volumetric flow rate per height [m^2/s]	w	channel width [m]
$\mathbf{Q_m}$	momentum flow rate per mass and height [m^3/s^2]	h	channel heigth [m]
Re_{D_h}	Reynolds number of flow based on the microchannel hydraulic diameter	ε	wall roughness [m]
		μ	dynamic viscosity [kg/ms]
Re_w	Reynolds number for a horizontal measurement plane	ν	kinematic viscosity [m^2/s]
u_i	velocity component in the x_i direction [m/s]	ρ	fluid density [kg/m^3]
u	velocity component in the streamwise direction [m/s]		
U	average streamwise velocity [m/s]		
v	crosswise velocity [m/s]		

relevant phenomena (e.g. surface roughness effects) – see e.g. Yu et al., 1995; Mala and Li, 1999; Qu et al., 2000; Pfund et al., 2000; Judy et al., 2002; Magueijo et al., 2006. On the other side, there are those claiming that the deviations found between microscale experiments and macroscale theory are due to measurement errors, such as unaccounted experimental uncertainties, incorrect characterization of the microchannels geometry, or overlooked entrance effects – see e.g. Sharp and Adrian, 2004; Celata et al., 2005; Kohl et al., 2005.

It should be stressed that most of the above-mentioned works were somehow limited as they were based on measurement techniques of bulk flow properties, such as the mass flow rate and the static pressure, referring to measurements obtained at plenums or reservoirs rather than at the channel itself. This flaw may be overcome by applying alternative techniques that allow for the detailed characterization of local flow properties. In fact, according to Sinton (2004), micro-Particle Image Velocimetry (micro-PIV) is the most promising visualization technique since it can produce high-quality results with spatial and temporal resolutions much higher than the remaining experimental techniques currently available.

The first micro-PIV application studying a Hele–Shaw flow with a cylindrical obstruction in the centre of a 120 μm square cross-section channel was presented by Santiago et al. (1998). The two-dimensional results were obtained with 6.9×6.9 μm spatial resolution in a single plane demonstrating the viability of using micro-PIV for micro-flows characterization. Meinhart et al. (1999), attaining a spatial resolution of 0.9×13.6 μm, extended the previous work to the measurement of velocities in a single plane for a flow inside a 30×300 μm glass channel, using for the first time an experimental setup similar to those presently in use. Sharp and Adrian (2004), using a Nd:YAG laser, a 12 bits CCD (charge coupled device) camera and tracing particles with diameters ranging from 3.8 to 19 μm, measured liquid flow velocities restricted to the central plane at numerous microtubes with circular cross-sections with diameters ranging from 50 to 247 μm.

In this work, the micro-PIV technique is used to characterize in detail the flow in a highly irregular microchannel as far as surface roughness is concerned. Such characterization aims at identifying possible surface phenomena that are usually not accounted for in macroscale flows. For that, it is developed herein a new method capable of quantifying the effect of walls surface roughness in microchannels flows, starting from measured velocities with micro-PIV. Moreover, such method is applicable to any geometry and any surface roughness of the walls, even to channels geometries where the flow governing equations lack of analytical solution, which are probably the vast majority of the practical cases. The present procedure is general for any fully developed flow. It should be mentioned that the previous works have compared experimental data against analytical solutions of the governing flow equations assuming well-behaved geometries (regular cross-sections, parallel walls, etc.) which, due to the manufacture technologies limitations, is not the case of most microchannels.

To accomplish the previous objective, two-dimensional velocity profiles are measured in 61 horizontal planes belonging to the same cross-sections of a microchannel allowing the reconstruction of the three-dimensional velocity profiles. Those three-dimensional velocity profiles are compared against three-dimensional CFD predictions referring to the same cross-section but possessing hydrodynamically smooth surfaces. Based on the yielded velocity data the Navier–Stokes equations are integrated and the Poiseuille number is computed both for the experimental and the numerical cases. The comparison of this parameter allows one to quantify the influence of surface roughness effects in a pressure-driven fully developed microfluidic flow. Moreover, an extensive error analysis to estimate the micro-PIV results accuracy is performed. First, the main error sources related to the micro-PIV technique are quantified. Then, the velocity profiles yielded by micro-PIV are integrated to calculate the volumetric flow rate and these results are compared to the overall measured flow. The differences can be used as standards of the micro-PIV data accuracy.

2. Experimental setup

In the present work is used a microchannel provided by DantecDynamics® with geometry schematically represented in Fig. 1. The rectilinear section of the microchannel enclosed by the ellipse drawn in the same figure is the region under study herein. The fluid used in all experiments is deionised water. The required pressure for the fluid to flow is provided by gravity through the height difference between two reservoirs. This height difference was chan-

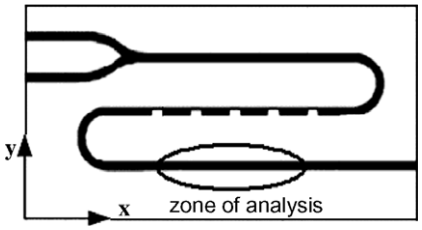

Fig. 1. Scheme of the studied microchannel integrated in a chip platform provided by DantecDynamics®.

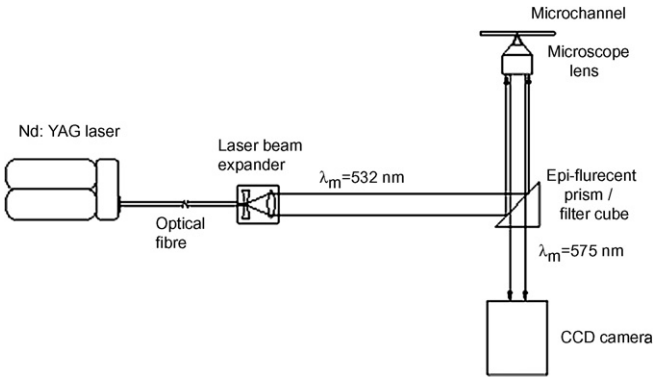

Fig. 2. Scheme of the DantecDynamics® assembled micro-PIV equipment.

ged whenever a change in the flow rate and, consequently, in the Reynolds number of the flow was required. The volumetric flow rate for a specific height difference was computed by measuring the volume discharged by the source reservoir (5 ml syringe) as a function of time.

The micro-PIV equipment (Fig. 2) assembled by DantecDynamics® consisted of a pulsed Nd:YAG laser New Wave® Solo II-15 (emitting at $\lambda_{exc} = 532$ nm); a fluorescent nile red flow-tracing particles with an average diameter of 1 μm; an epi-fluorescent prism (filter cube), used to filter out background noise allowing only the red light, emitted by the fluorescent tracing particles ($\lambda_{em} = 575$ nm), to reach the camera; and a Flowsense® 2M CCD camera providing an image field of 1600×1186 pixels (pixel size = 7.4 μm) at maximum repetition rate of 15 Hz and 8/10-bit intensity resolution. To get a magnified field of view the camera is coupled to a Leica® DM ILM epi-fluorescent microscope. The objective lens used are two, air-immersion, long working distance lens with magnifications of $M = 5$ and $M = 10$ and corresponding numerical apertures of NA = 0.12 and NA = 0.25, respectively.

Taking into account the kinematic properties of the flow under study and viewing the optimization of the signal-to-noise ratio, a time delay between laser pulses ranging from 100 to 500 μs and a repetition rate of 15 Hz are used to have a maximum particles displacement of approximately ¼ of the interrogation area length. Regarding the in-plane spatial resolution, interrogation areas of 64×64 pixels are used with 50% overlap in both streamwise and crosswise directions. Hence, a distance between individual vectors of 23.4×23.4 μm^2 was obtained, as depicted in Fig. 3. To increase the yielded vector maps reliability a time average correlation algorithm (Meinhart et al., 2000) is applied over 100 correlation maps.

3. Experimental techniques and related error sources

3.1. Micro-PIV technique

PIV is a non-intrusive optical technique used to measure the kinematic parameters of fluid flows. With this technique the flow velocity is determined by measuring the displacement of a collection of seeding particles between two recorded images separated by a known period of time. Each image is divided into a certain number of cells, the interrogation areas, each containing a certain amount of particles. For traditional cross-correlation algorithms a minimum of five particles per interrogation area is usually required. For more advanced correlation algorithms (e.g. ensemble time average correlation algorithms) this requirement may not be necessary as demonstrated by Meinhart et al. (2000). The average displacement of the amount of particles contained in each interrogation area is determined by means of a cross-correlation process between the two recorded images. Velocity vectors are obtained by dividing the particles displacement by the time interval between the two frames. Micro-PIV is a technique based on the

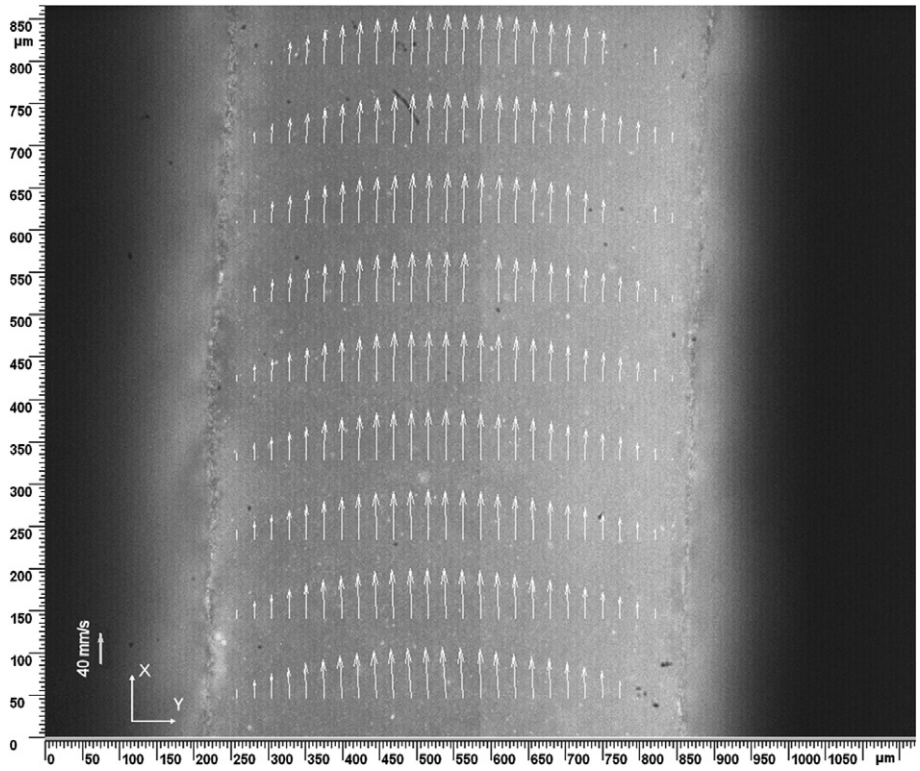

Fig. 3. Example of an image of the studied microchannel rectilinear section at a horizontal plane with measured velocity vectors.

PIV concept. However, since micro-PIV is applied to studies where much higher resolutions are required, there are a few differences between both techniques. Wereley et al. (2002) outlined three main aspects that differentiate micro-PIV from traditional PIV. First, instead of using a laser light sheet the flow field is volume illuminated. As a result, when seeding concentration is too high the background noise from out-of-focus particles will have a high intensity. Secondly, the use of particles smaller than laser light wavelength invalidates the employment of light scattering techniques. This situation occurs when spatial resolutions of only a few microns, or even nanometres, are required. Finally, Brownian motion effects on particles with diameters smaller than 1 μm may play an important role in determining the velocity of particles following the flow since that introduces an additional percentage of uncertainty in the final result.

3.2. Error sources

The experimental nature of this micro-PIV study may affect the results with several error sources. Considering the complexity of quantifying *a priori* all the error sources, only the most relevant ones will be briefly analysed. A more detailed analysis can be found in the work of Silva (2006).

A primary error source is related to inertial effects between the particles displacement and the fluid motion. Based on a simple Stokes drag-law analysis, as suggested by Raffael et al. (1998), the time lag response for a particle immersed in a flow at rest and suddenly set into constant acceleration is 10^{-8} s. Since the characteristic time scale of the present flow, defined by the time interval between two consecutive laser pulses, $\Delta t_{\text{pulse}} \approx 10^{-4}$ s, is several orders of magnitude larger than 10^{-8} s, the error due to the inertial effects of particles is negligible. At sub-micron scales Brownian motion can assume a significant influence in the physical description of the tracer particles motion (Devasenathipathy et al., 2003). For the present case, where tracer particles mean diameter is $d_p = 1$ μm, and their displacement is computed through an ensemble time-average algorithm, Brownian motion effects have a negligible influence. For a cross-correlation algorithm the in-plane velocity is computed by locating the highest peak in the correlation plane. The uncertainty in locating this correlation peak is closely related to the particles image size (d_e). Therefore, as demonstrated by Prasad et al. (1992), as long as d_e is resolved by 3 to 4 pixels, the uncertainty in locating the correlation peak and thus in computing the in-plane velocity can be estimated as $d_e/10$ M. Since $d_e/10$ M = 0.30 μm is about two orders of magnitude smaller than the characteristic flow length-scale, chosen herein as the distance between individual velocity vectors, i.e. 23.4 μm which approximates the interrogation area length-scale, this uncertainty does not influence significantly the in-plane velocity results. The presence of out-of-plane particles contributing to the in-plane velocity can bias the computation of the latter if the measurement volume is too thick and strong velocity gradients in the out-of-plane direction exist simultaneously. Using the methodology presented by Olsen and Adrian (2000), the measurement volume thickness, given by the depth of correlation, was estimated to be 36.8 μm. Considering the depth of the microchannel, approximately 910 μm, and the velocity profile of the flow along the depth direction, the thickness of the measurement volume employed is not expected to have considerable influence in the overall accuracy of the in-plane results.

Although the previous *a priori* analysis suggests that the error sources previously reported have negligible influence on the accuracy of measurements presented herein, a more thorough analysis is carried out to compute the global accuracy of the micro-PIV results. The procedure adopted consists in computing, for a fixed streamwise flow location ($X = 200$ μm, see Fig. 3), the value of the volumetric flow rate yielded by the volumetric integral enclosing 61 two-dimensional velocity profiles obtained through micro-PIV measurements. This process is then repeated for two other streamwise flow locations further downstream ($X = 400$ μm and $X = 700$ μm in Fig. 3). The results are compared against the measured volumetric flow rate discharged to the sink reservoir, hereafter designated as theoretical flow rate. It should be noted that in all experiments the pressure head is always the same. For the present study, the theoretical volumetric flow rate is 1.05 ml/min ±2.5%, whereas the corresponding value computed through micro-PIV data is 1.01 ml/min ±1.5%, which gives a difference in flow rates of ca. 3%. This last value provides an indication of the order of magnitude of the micro-PIV technique bias error. Any measured phenomenon whose magnitude is above this threshold is relevant, i.e. it is considered not to be generated by experimental uncertainties.

4. Microchannel geometry and flow characterization

4.1. Flow physical modelling

The mass and momentum balance equations, i.e. the continuity and the Navier–Stokes equations, for a steady, laminar and incompressible flow of a Newtonian fluid with constant properties are expressed by the following equations

$$\frac{\partial u_i}{\partial x_i} = 0, \tag{1}$$

$$u_j \frac{\partial u_i}{\partial x_j} = -\frac{1}{\rho}\frac{\partial p}{\partial x_i} + \nu\left(\frac{\partial^2 u_i}{\partial x_j^2}\right), \tag{2}$$

where u_i represents the velocity component in the i direction, p is the pressure, ρ is the fluid density and ν is the kinematic viscosity. The fluid properties are evaluated at the operating temperature of 293 K.

Since the flow is driven by a pressure head yielded by the height difference between a source and a sink reservoir, the steady flow condition needs to be analysed. The change in the pressure head, given by the change of the liquid heights in the reservoirs, is observed throughout the time for each analysis (time required to capture the ensemble of images). Considering the reservoirs size (5 ml syringes with 12 mm of diameter) and the characteristic time interval of each analysis ($\Delta t = 5$ s), the change in liquid height between reservoirs was 0.7 mm, which corresponds to a static pressure head of less than 0.7 Pa. This minimal variation of the microchannel inlet/outlet pressure difference is irrelevant, i.e. it is less than 1.7% of the total pressure head value responsible for the fluid flow and, consequently, its value can be considered as constant in time.

The laminar characteristic of the microflow was verified by estimating its Reynolds number. As the largest volumetric flow rate was $Q = 1.5$ ml/min the corresponding largest Reynolds number based on the microchannel hydraulic diameter, $D_h = 637$ μm, computed from $Re_{D_h} = 4Q/(\pi \nu D_h)$, is 50. This small Reynolds number value determines undoubtedly the flow regime as laminar.

4.2. Analysis of the microchannel cross-section and CFD modelling

Experimental data evidences a parabolic form of the horizontal velocity profiles. Hence, the experimental velocity profiles are fitted to parabolas. The roots of those fitted parabolas are extracted and their values are associated with the walls locations on the microchannel using the no-slip velocity boundary condition. The use of this approach allowed for the definition of the channel cross-section with accuracy up to 10 times higher than that of visual inspection (given by the image pixel size) – see Silva (2006).

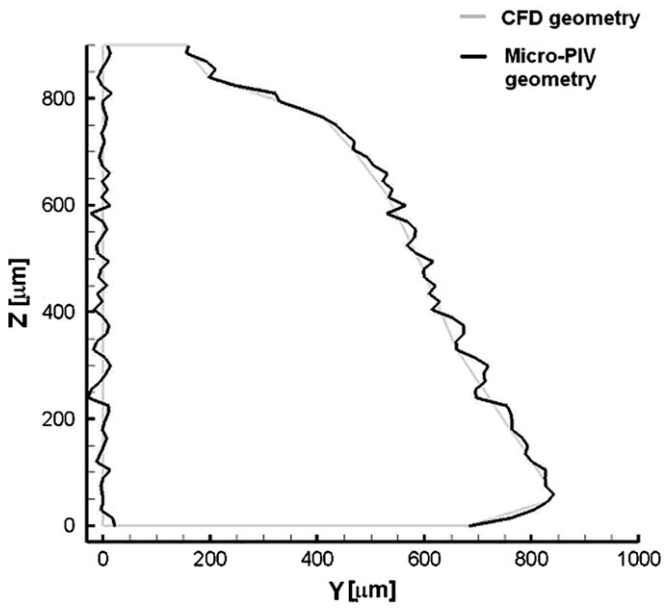

Fig. 4. The microchannel cross-section geometry.

This procedure yielded dimensions of approximately 910 μm height and width between ca. 843 μm and ca. 142 μm at the bottom and at the top regions, respectively. The microchannel cross-section has the shape displayed Fig. 4. Based on the cross-section obtained with micro-PIV a similar geometry was generated using Gambit® 2.2.30 with the mesh generator code used in the present CFD study. As observed from Fig. 4, the difference between the two geometries lies on the smoothness of the CFD surface that contrasts significantly with the roughness of the actual channel. This value is estimated as the standard deviation between the sawtooth type experimental cross-section and the smooth CFD geometry, which, in average, is 10.2 μm for the right-hand side of the channel and 10.5 μm for the left-hand side. Such values yield a relative roughness value referred to the microchannel hydraulic diameter of $\varepsilon/D_h \approx 1.6\%$. Roughness values at the top and bottom walls could not be quantified because measurements in these regions are severely limited by optical constrains. Because of that, it is assumed in this work that those walls possess the same roughness values. Moreover, wall irregularities along the microchannel streamwise flow direction (*xx* direction in Fig. 3) are not considered in the CFD model.

For the sake of accuracy and computational efficiency, a structured mesh with around 3×10^5 hexahedron elements was used in the domain discretization, imposing control volumes sizes equal to those of the micro-PIV measurements. The numerical simulations were performed with FLUENT® 6.2.16. The flow field was modelled as steady and laminar Eqs. (1) and (2), and the inlet/outlet boundary conditions were set as mass flow inlet and outflow, respectively. The mass flow inlet value was set to a value of 1.75×10^{-5} kg/s that corresponds to the volumetric flow rate of 1.05 ml/min. The no-slip velocity condition at solid boundaries was applied to all the microchannel walls.

4.3. Analysis of the fully developed flow condition

As stated before, the micro-PIV technique provides a two-dimensional velocity field for each measurement. Therefore, the three-dimensional velocity profile had to be built up by measuring 61 horizontal planes over the microchannel height. Fig. 5a displays the micro-PIV results. The CFD three-dimensional velocity profile

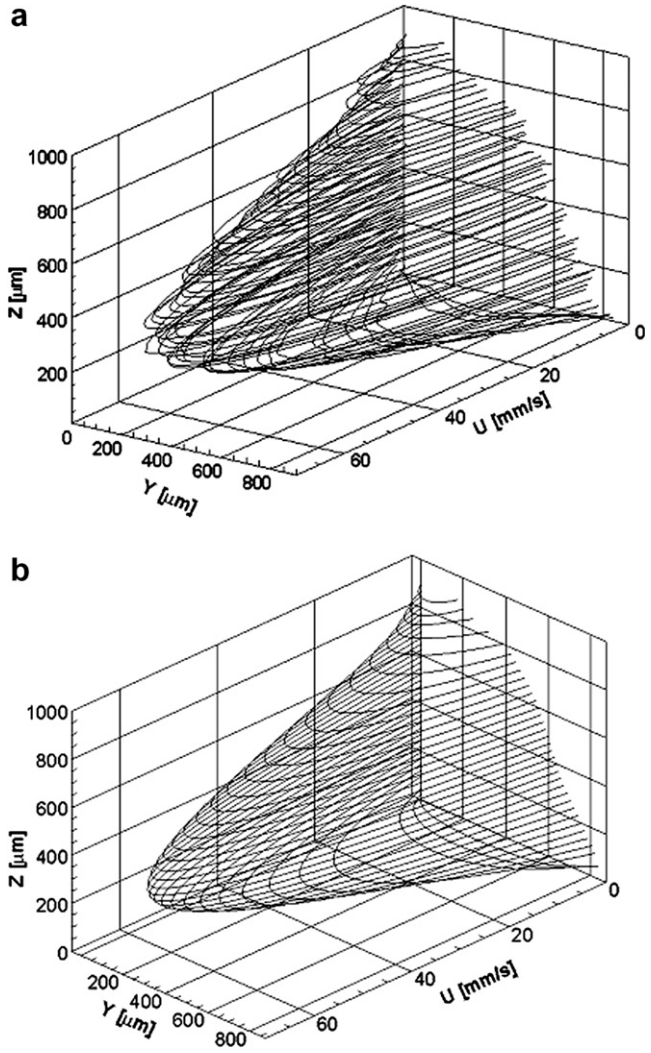

Fig. 5. Measured and computed velocity profiles in the microchannel rectilinear section. (a) Micro-PIV two-dimensional measurements in 63 horizontal planes. (b) CFD three-dimensional calculations.

was computed following a similar procedure and the results are shown in Fig. 5b. As reported before, the volumetric flow rate found by volumetric integration of the velocity profiles yielded by micro-PIV measurements (Fig. 5a) fits with the theoretical value within a deviation of 3%, which provides an order of magnitude of the micro-PIV technique bias error. Therefore, if the computation of the momentum flow rate imbalance yields values within this 3% uncertainty, the convective term in Eq. (2) $u_j \frac{\partial u_i}{\partial x_j}$, can be set to zero and the flow considered as fully developed. The volumetric flow rate per unit height, *Q*, and the momentum flow rate per unit mass and height, $\mathbf{Q_m}$, are computed as follows:

$$Q = \int (\mathbf{V} \cdot \mathbf{n}) dy \approx \sum (u_{i+1} + u_i)(y_{i+1} - y_i)/2, \tag{3}$$

$$\mathbf{Q_m} = \int (\mathbf{V} \cdot \mathbf{n}) \cdot \mathbf{V} dy \approx \sum (u_{i+1}^2 + u_i^2)(y_{i+1} - y_i)/2. \tag{4}$$

In the previous equations the index *i* denote the interrogation area (or measurement volume) where the relevant variables are being referred to; y_i refers to the location of the interrogation area centroid *i* and u_i refers to the corresponding velocity component computed in the same interrogation area *i*.

Fig. 6 depicts several velocity profiles at different streamwise flow locations at the same measurement plane for a constant Rey-

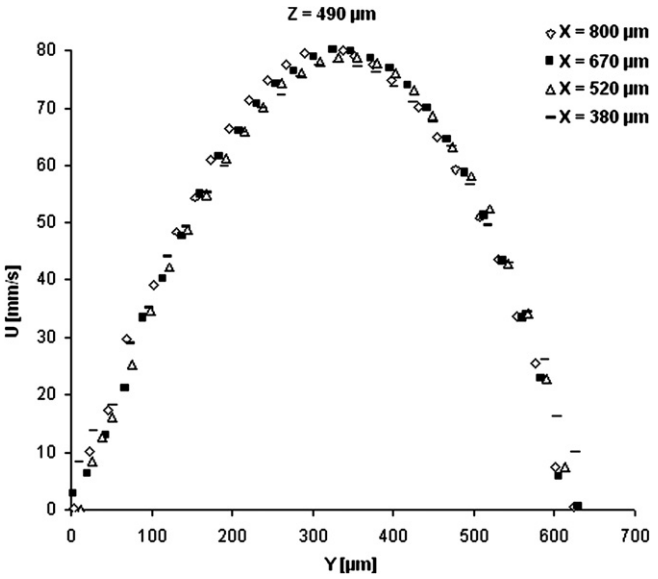

Fig. 6. Measured velocity profiles $u(y)$ at different streamwise flow locations ($X = 380$ μm; $X = 520$ μm; $X = 670$ μm; $X = 800$ μm) for $Re_w = 31$, $Re_w = \frac{Uw}{\nu}$.

Table 1
Volumetric flow rates per unit height, Q_v, momentum flow rates per unit height and mass, $\mathbf{Q_m}$, and corresponding errors (ΔQ_v and $\Delta\mathbf{Q_m}$) for $Re_w = 39$, $Re_w = 31$, $Re_w = 20$, $Re_w = Uw/\nu$, at different streamwise flow positions and at a channel height of $Z = 225$ μm

Position	Q_v (cm^2/s)	$\mathbf{Q_m}$ (cm^3/s^2)	ΔQ_v (%)	$\Delta\mathbf{Q_m}$ (%)
$Re_w = 39$				
$X = 60$ μm	39.95	268.98	0.00	0.00
$X = 200$ μm	39.68	267.10	0.67	0.70
$X = 400$ μm	39.36	262.96	0.80	1.55
$X = 600$ μm	39.33	258.02	0.08	1.88
$X = 800$ μm	38.92	251.07	1.04	2.69
$Re_w = 31$				
$X = 50$ μm	31.69	168.44	0.00	0.00
$X = 200$ μm	31.40	167.56	0.91	0.53
$X = 350$ μm	31.31	166.08	0.30	0.88
$X = 550$ μm	31.15	161.81	0.52	2.57
$X = 700$ μm	30.82	158.70	1.06	1.93
$Re_w = 20$				
$X = 75$ μm	20.31	69.70	0.00	0.00
$X = 200$ μm	20.15	69.01	0.78	1.00
$X = 300$ μm	20.16	68.39	0.04	0.90
$X = 500$ μm	20.11	67.30	0.26	1.59
$X = 700$ μm	19.70	65.08	1.99	3.29

nolds number, $Re_w = 31$. As it can be observed velocity profiles practically overlap. This allows one to infer that the imbalances of Q_v and $\mathbf{Q_m}$ in the streamwise flow direction are practically nil, and this can be confirmed by the quantification performed and shown in Table 1. The Reynolds number in this case is defined as $Re_w = Uw/\nu$ where U refers to the average velocity of the flow in the measurement plane and w represents the width of the channel in the measurement plane. As it can be observed from Table 1 the maximum value of the volumetric flow rate imbalance per unit height (ΔQ_v) in the horizontal plane under study ($Z = 225$ μm) is less than 2% whereas the maximum value found for the momentum flow rate imbalance per unit mass and height ($\Delta\mathbf{Q_m}$) is 3.3%. The value of ΔQ_m is larger than that of ΔQ_v because the former is affected by the latter. Therefore, its actual intrinsic value is considerably smaller (approximately of the same order of magnitude of ΔQ_v). Since these values are within the measurements uncertainty, 3%, one may consider the flow to be fully developed, at least at the measurement plane under analysis. Extending this same study to the entire three-dimensional flow field (see Fig. 5a) the momentum flow rate imbalance computed for $Re_{D_h} = 34$, where the Reynolds number is based on the channel hydraulic diameter, along three distinctive axial directions ($X = 200$ μm, $X = 400$ μm and $X = 700$ μm, displayed in Fig. 3) is 3.4%. Since the maximum volumetric flow rate imbalance among the three distinctive axial locations was 1.5%, the corresponding intrinsic value of the momentum flow rate imbalance is smaller and within the 3% uncertainty. Hence, the fully developed condition in the whole flow field is expressed by the following equation

$$\partial p/\partial x = \mu\left(\frac{\partial^2 u}{\partial y^2} + \frac{\partial^2 u}{\partial z^2}\right). \tag{5}$$

Eq. (5) is the simplest form of the Navier–Stokes equation for a flow of the type studied herein. Despite its simplicity, analytical solutions are limited to particular channel cross-sectional geometries (Shah and London, 1978). If the channel geometry is characterized by an irregular cross-section with a non analytical shape, as it commonly happens for microgeometries, flow field solutions can only be obtained by employing numerical tools as CFD, as in the case studied herein – see Fig. 4. Therefore, the assessment of possible microfluidic departures from traditional macroscale theory is performed by comparing the micro-PIV experimental data against similar data yielded by a numerical model in a smooth walls geometry, where the traditional macroscale Navier–Stokes equations are employed – Eqs. (1) and (2).

5. Results and discussion

5.1. Measured and predicted velocity profiles

Fig. 7 shows the measured and predicted velocity profiles for identical flow rates as a function of the channel width (in the *yy* direction) for a streamwise location where the fully developed condition is verified at four distinct channel heights: $Z = 50$ μm, $Z = 150$ μm, $Z = 775$ μm and $Z = 850$ μm. These planes were chosen intentionally to show the effects of the top and bottom walls roughness on the velocity profiles when compared to CFD predictions on the same geometry but with smooth walls. In fact, the closer to the top and bottom walls the velocity profiles are, the larger is the influence of their roughness on the velocity profiles, and this is confirmed by the results. Besides observing that micro-PIV velocity profiles exhibit higher strain rates near the wall than those predicted by CFD, it is also noticed that the micro-PIV velocities at the regions of both the top ($Z = 50$ μm and $Z = 150$ μm) and bottom ($Z = 775$ μm and $Z = 850$ μm) walls have a much larger magnitude. Hence, the experimental velocity profile along the channel height (in the *zz* direction) is also expected to have a much higher strain rate than the numerical one. Furthermore, it is observed that the predicted maximum velocity locations are markedly deviated to smaller Y values than those of the measured ones. Since the CFD predictions are performed for the same conditions as those existing in the experimental setup, apart from the smooth walls assumption, and these flow regions close to walls are the more affected ones, it can be inferred that such differences are caused by the wall roughness.

Fig. 8 exhibits measured and predicted velocity profiles for the same conditions as those of Fig. 7 at six different channel heights away from the top and bottom walls: $Z = 300$ μm, $Z = 375$ μm, $Z = 450$ μm, $Z = 500$ μm, $Z = 650$ μm, and $Z = 675$ μm. For this situation, the numerical and experimental results are in much better agreement. Even though, the measured velocity profiles still exhibit larger strain rates near the walls but, in

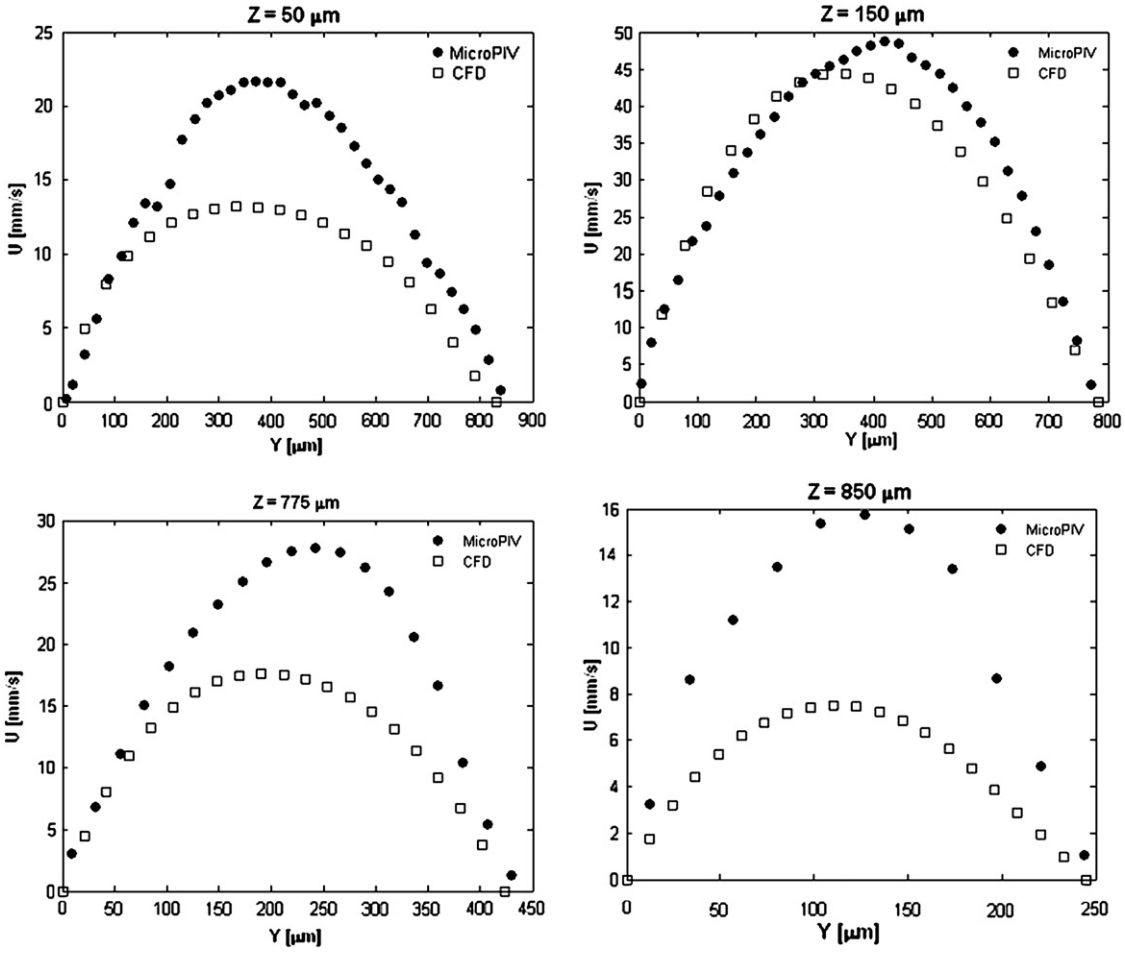

Fig. 7. Measured and predicted velocity profiles $u(y)$ for fully developed flow at $Z = 50$ μm; $Z = 150$ μm; $Z = 775$ μm; $Z = 850$ μm.

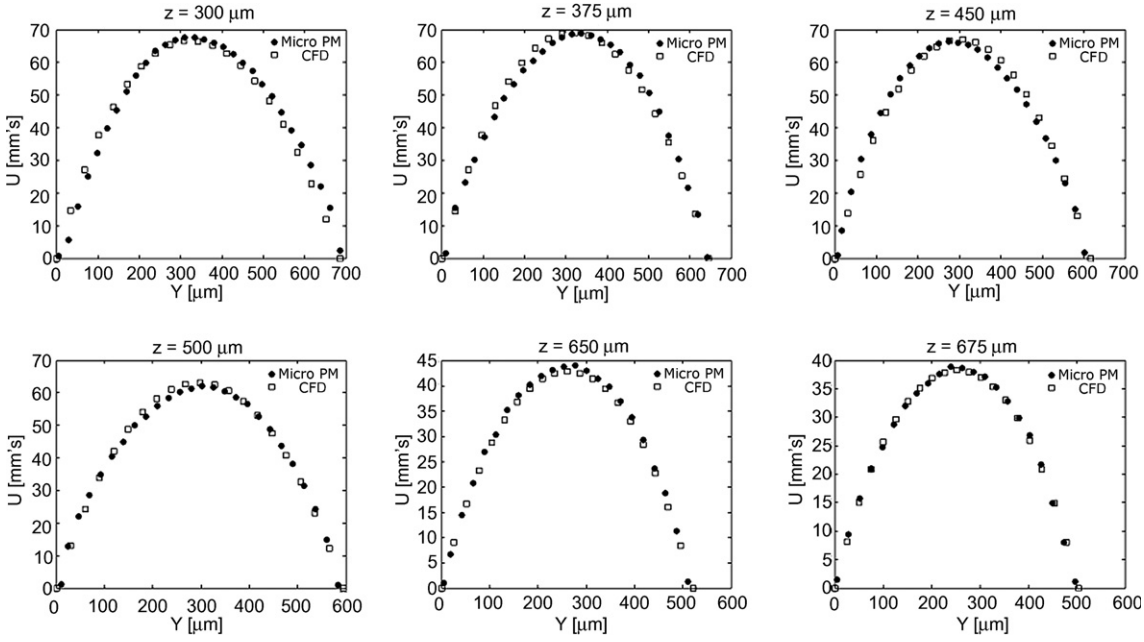

Fig. 8. Measured and predicted velocity profiles $u(y)$ for fully developed flow at $Z = 300$ μm; $Z = 375$ μm; $Z = 450$ μm; $Z = 500$ μm; $Z = 650$ μm; $Z = 675$ μm.

opposition to that occurred close to the near top/bottom walls, the numerical velocities have larger magnitudes, very similar to the experimental ones.

To ascertain the influence of the surface roughness on the streamwise flow direction, recourse was made to the information provided by the isovelocity contour plots. Fig. 9a and b depict

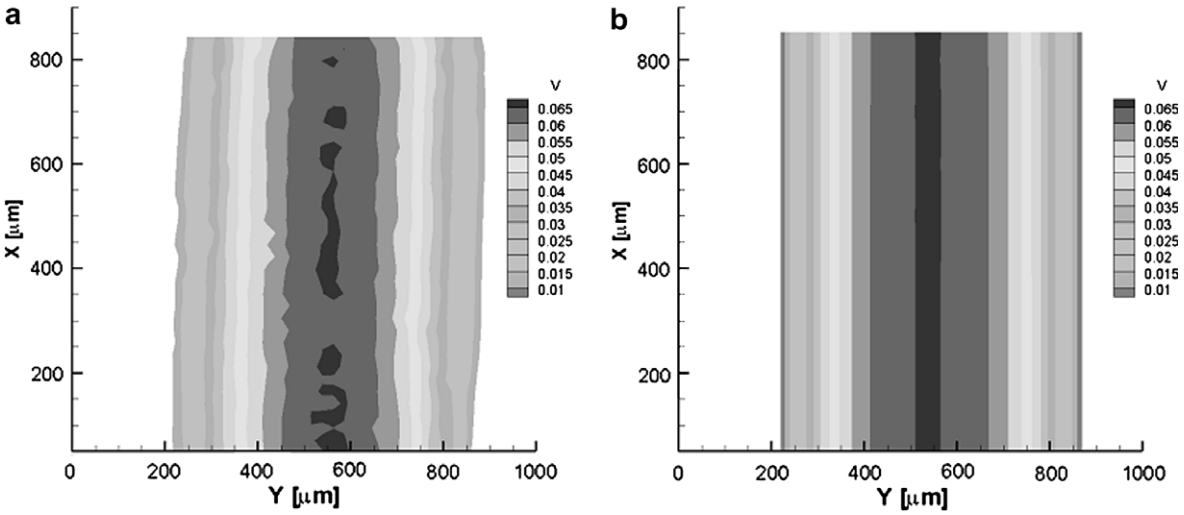

Fig. 9. Isovelocity contour plots at $Z = 450$ μm. (a) Micro-PIV experimental values. (b) CFD predicted values.

two isovelocity contour plots for a horizontal plane at mid-height (Z = 450 μm) for $Re_w = 20$. As it can be observed in Fig. 9a rather than developing parallel to each other, as it occurs with those predicted by CFD (Fig. 9b), the regions of constant velocity experience some meander pattern and even discontinuities due to surface roughness. The presence of discontinuities in the core region of the microchannel allows one to verify the important dependency of the fluid flow pattern on the local walls irregularities. Local contractions and expansions in the channel walls promote local accelerations and decelerations that lead the fluid motion to follow the walls irregularities in the streamwise flow direction.

Since the results above discussed refer to a fixed Reynolds number it is mandatory to verify the influence of this parameter on the yielded results. For that, the level between pressure heads was

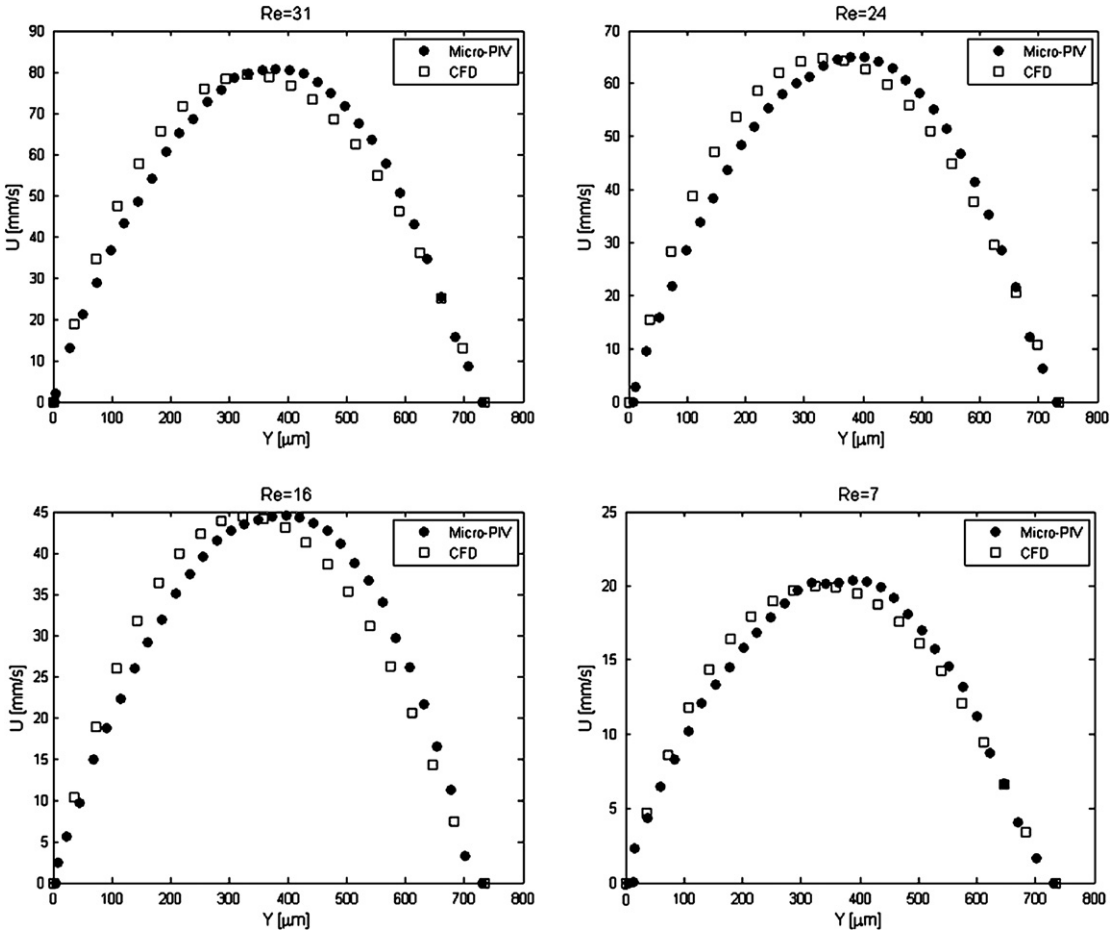

Fig. 10. Measured and predicted velocity profiles $u(y)$ for fully developed flow at $Z = 225$ μm for $Re_w = 31$, $Re_w = 24$ and for $Re_w = 16$, $Re_w = \frac{Uw}{\nu}$.

changed making possible the measurement of the flow field for several Reynolds number values, which are defined as $Re_w = Uw/\nu$. Fig. 10 depicts the results obtained at the plane $Z = 225$ μm. As it can be observed, the same reasoning is applied independently of the Reynolds number value. In fact, the velocity profiles at the same position ($Z = 225$ μm) exhibit the same pattern.

5.2. Poiseuille number calculations

The previous study allowed one to infer and verify that the surface roughness influences the flow field pattern in the three coordinate directions. In order to quantify such influence, the friction factor values, i.e. the Poiseuille numbers, $\mathrm{Po} \equiv fRe$, were computed both for experimental and numerical cases. In this study, it is used the Fanning friction factor definition: $f \equiv \frac{D_h}{1/2\rho U^2}|\partial p/\partial x|$. Since it is required the knowledge of the pressure drop term, $\partial p/\partial x$, and the micro-PIV technique only provides kinematic data, Eq. (5) needs to be integrated. The control volume used in this integration process encloses the whole microchannel cross-section

$$\iiint \partial p/\partial x \,\mathrm{d}x\,\mathrm{d}y\,\mathrm{d}z = \iiint \mu\left(\frac{\partial^2 u}{\partial y^2} + \frac{\partial^2 u}{\partial z^2}\right)\mathrm{d}x\,\mathrm{d}y\,\mathrm{d}z. \tag{6}$$

Taking into account that the fully developed flow establishes that $\partial p/\partial x$ is constant and all the kinematic variables inside the integrals of Eq. (6) are independent of x, one obtains:

$$\frac{\mathrm{d}p}{\mathrm{d}x}\int_0^{h(y)}\int_0^{w(z)}\mathrm{d}y\,\mathrm{d}z = \int_0^{h(y)}\mu\left(\left.\frac{\partial u}{\partial y}\right|_{w(z)} - \left.\frac{\partial u}{\partial y}\right|_0\right)\mathrm{d}z + \int_0^{w(z)}\mu\left(\left.\frac{\partial u}{\partial z}\right|_{h(y)} - \left.\frac{\partial u}{\partial z}\right|_0\right)\mathrm{d}y, \tag{7}$$

where in the above equation w is the microchannel width and h the microchannel height.

Taking into account both micro-PIV and CFD methods yield discrete velocity data, the integrals present in Eq. (7) are approximated by sums as expressed by the following equation

$$\frac{\mathrm{d}p}{\mathrm{d}x} = \frac{1}{\sum_{j=1}^{M}\Delta y_j}\left[\frac{1}{\sum_{i=1}^{N}\Delta z_i}\sum_{i=1}^{N}\mu\left(\left.\frac{\partial u}{\partial y}\right|_{w(z_i)} - \left.\frac{\partial u}{\partial y}\right|_0\right)_i \Delta z_i\right] + \frac{1}{\sum_{i=1}^{N}\Delta z_i}\left[\frac{1}{\sum_{j=1}^{M}\Delta y_j}\sum_{j=1}^{M}\mu\left(\left.\frac{\partial u}{\partial z}\right|_{H(y_j)} - \left.\frac{\partial u}{\partial z}\right|_0\right)_j \Delta y_j\right]. \tag{8}$$

In the above equation, N is the number of measurement planes and Δz is the vertical distance between horizontal planes. Similarly, M is the number of vertical planes crossing a horizontal measurement plane and Δy is the horizontal distance between vertical planes.

If a significant number of measurement data is taken into consideration it is expected that the sum converges to a finite bounded value, which is the value of the integral. Table 2 displays the values of those sums for the experimental and predicted results, which are considered to be converged since limitations of the micro-PIV interrogation volumes do not allow the use of smaller values for Δy and Δz. It should be mentioned that the wall shear stresses are calculated from the velocity derivative values at the walls obtained from both the experimental velocity profiles and the predicted ones. Since the micro-PIV error quantification is performed considering the entire flow field, the shear stresses calculation must also be based on the same data. Therefore, parabolic profiles were fitted to both experimental and CFD data and this allows for a straightforward estimation of the velocity derivatives in Eq. (8).

Table 2
Values of the right-hand side terms of Eq. (8) computed for $Re_{D_h} = 34$

	Experimental	CFD
$\frac{1}{\sum_{j=1}^{M}\Delta y_j}\left[\frac{1}{\sum_{i=1}^{N}\Delta z_i}\sum_{i=1}^{N}\mu\left(\left.\frac{\partial u}{\partial y}\right\|_{w(z_i)} - \left.\frac{\partial u}{\partial y}\right\|_0\right)_i \Delta z_i\right]$	−1702.8	−1459.0
$\frac{1}{\sum_{i=1}^{N}\Delta z_i}\left[\frac{1}{\sum_{j=1}^{M}\Delta y_j}\sum_{j=1}^{M}\mu\left(\left.\frac{\partial u}{\partial z}\right\|_{h(y_j)} - \left.\frac{\partial u}{\partial z}\right\|_0\right)_j \Delta y_j\right]$	−1242.6	−1191.8

Table 3
Friction factor, f, and Poiseuille number, Po, computations for experimental and numerical predictions for $Re_{D_h} = 34$

	Experimental	CFD
$\mathrm{d}p/\mathrm{d}x$	−1473	−1325
f	0.62	0.56
Po	21.8	19.6

For the Reynolds number under study, i.e. $\mathrm{Re}_{D_h} = 34$, the difference between Poiseuille numbers (Table 3) was found to be ca. 11% ($\mathrm{Po}_{exp} = 21.8$ vs. $\mathrm{Po}_{CFD} = 19.6$) whereas the estimated uncertainty of this analysis is 4.5% (see Section 5.3). The 11% difference between the micro-PIV experimental values and the corresponding predicted Poiseuille number quantifies the amount of momentum in excess to the smooth surface that a laminar microfluidic flow experiences due to surface roughness effects.

5.3. Associated errors

All physical parameters present in this study are obtainable: the volumetric flow rate value Q may be given by the volume enclosed by the velocity profiles; the pressure gradient $\mathrm{d}p/\mathrm{d}x$ may be given by the integration of the Navier–Stokes equation; and the channel hydraulic diameter D_h may be given by the channel cross-section dimensions determined through the procedure adopted to estimate the walls location, Silva (2006). Therefore, the computation of the uncertainties present in the remaining parameters follows the equations expressed below.

The average velocity uncertainty $\delta(U)$ is given by:

$$\delta U = \left[\left(\frac{\delta(Q)}{D_h}\right)^2 + \left(-\frac{Q}{D_h^2}\delta(D_h)\right)^2\right]^{\frac{1}{2}}. \tag{9}$$

The Poiseuille number uncertainty $\delta(\mathrm{Po})$ is computed as:

$$\delta(\mathrm{Po}) = \left[\begin{array}{l}\left(2\frac{(D_h)^2}{\mu U}\delta\left(\frac{\mathrm{d}p}{\mathrm{d}x}\right)\right)^2 + \left(4\left(\frac{\mathrm{d}p}{\mathrm{d}x}\right)\frac{D_h}{\mu U}\delta(D_h)\right)^2 + \\ \left(-2\left(\frac{\mathrm{d}p}{\mathrm{d}x}\right)\frac{(D_h)^2}{\mu U^2}\delta(U)\right)^2\end{array}\right]^{\frac{1}{2}}. \tag{10}$$

In the previous equation $\delta(\mathrm{d}p/\mathrm{d}x)$ reflects the error produced by fitting the velocity profiles to parabolas and has a value of 4.4%, $\delta(D_h)$ quantifies the uncertainty in determining the microchannel hydraulic diameter as described in Silva (2006) and has a negligible influence in this case, and $\delta(U)$ quantifies the estimated uncertainty of the micro-PIV velocity values that, as explained before, has a value of 3%.

6. Conclusions

In this work was confirmed the effective influence of the surface roughness on the laminar microscopic liquid flows behaviour. For that, data measured with micro-PIV were compared against CFD predictions for similar conditions but, in order to quantify the wall roughness effects, the numerical predictions were performed for a hydrodynamically smooth geometry. This contrasts with the measured relative roughness value of $\varepsilon/D_h \approx 1.6\%$ for the experimental case. Since micro-PIV provides only two-dimensional velocity data, 61 planes along the microchannel cross-section were used for velocity measurements allowing the reconstruction of the

three-dimensional velocity profiles. To evaluate the results accuracy, the micro-PIV volumetric flow rate, yielded by the volume enclosed by the 61 two-dimensional velocity profiles, was compared against a theoretical value, here defined as the volume of fluid discharged to the sink reservoir as a function of time. The difference was estimated to be 3%, which provides an indication of the bias error of the global micro-PIV measurements. Similarly, the momentum flow rate, based on the same experimental data, was computed and the results proved the fully developed condition in the flow region under study. The experimental data, velocity profiles and isovelocity contour plots, evidenced the effects produced by the wall roughness on the flow. To quantify this, the Navier–Stokes equations for fully-developed flows were integrated using both the experimental data and the CFD predictions. Results showed that the non-consideration of the wall roughness for the conditions under study yield a friction factor underestimation in 11%.

Acknowledgment

The authors acknowledge the financial support given by *Fundação para a Ciência e Tecnologia* through the research project PTDC/EME-MFE/64566/2006.

References

Bayraktar, T., Pidugu, S., 2006. Characterization of liquid flows in microfluidic systems. Int. J. Heat Mass Trans. 49, 815–824.

Celata, G., Cumo, M., McPhail, S., Zummo, G., 2005. Characterization of fluid dynamic behaviour and channel wall effects in microtube. Int. J. Heat Fluid Flow 27, 135–143.

Devasenathipathy, S., Santiago, J., Wereley, S., Meinhart, C., Takehara, K., 2003. Particle imaging techniques for microfabricated fluidic systems. Exp. Fluids 34, 504–515.

Gad-el-Hak, M., 1999. The fluid mechanics of microdevices – the Freeman Scholar lecture. J. Fluids Eng. 121, 5–33.

Hetsroni, G., Mosyak, A., Pogrebnyak, E., Yarin, L., 2005. Fluid flow in microchannels. Int. J. Heat Mass Trans. 48, 1982–1998.

Judy, J., Maynes, D., Webb, B., 2002. Characterization of frictional pressure drop for liquid flows through microchannels. Int. J. Heat Mass Trans. 45, 3477–3489.

Kohl, M., Abdel-Khalik, S., Jeter, S., Sadowski, D., 2005. An experimental investigation of microchannel flow with internal pressure measurements. Int. J. Heat Mass Trans. 48, 1518–1533.

Magueijo, V., Semiao, V., Pinho, M.N., 2006. Effects of ultrafiltration permeation rates on the hydrodynamics of a minichannel/slit laminar flow. Chem. Eng. Sci. 61, 7139–7150.

Mala, G.M., Li, D., 1999. Flow characteristics of water in microtubes. Int. J. Heat Fluid Flow 20, 142–148.

Meinhart, C., Wereley, S., Santiago, J., 1999. PIV measurements of a microchannel flow. Exp. Fluids 27, 414–419.

Meinhart, C., Wereley, S., Santiago, J., 2000. A PIV algorithm for estimating time-average velocity fields. J. Fluids Eng. 122, 285–289.

Olsen, M., Adrian, R., 2000. Out-of-focus effects on particle image visibility and correlation in microscopic particle image velocimetry. Exp. Fluids 29, 166–174.

Pfund, D., Rector, D., Shekarriz, A., 2000. Pressure drop measurements in a microchannel. AICHE J. 46, 1496–1507.

Prasad, A., Adrian, R., Landreth, C., Offutt, P., 1992. Effect of resolution on the speed and accuracy of particle image velocimetry interrogation. Exp. Fluids 13, 105–116.

Qu, W., Mala, G., Li, D., 2000. Pressure-driven water flows in trapezoidal silicon microchannels. Int. J. Heat Mass Trans. 43, 353–364.

Raffael, M., Willert, C., Kompenhans, J., 1998. Particle Image Velocimetry – A Practical Guide. Springer.

Santiago, J., Wereley, S., Meinhart, C., Beebe, D., Adrian, R., 1998. A particle image velocimetry system for microfluidics. Exp. Fluids 25, 316–319.

Shah, R., London, A., 1978. Laminar flow forced convection in ducts. Advances in Heat Transfer, Supp. 1. Academic Press, New York.

Sharp, K., Adrian, R., 2004. Transition from laminar to turbulent flow in liquid filled microtubes. Exp. Fluids 36, 741–747.

Silva, G., 2006. Caracterização experimental de um escoamento microfluídico (Experimental Characterization of a Microfluidic Flow, in Portuguese), Graduation Thesis, Mechanical Engineering Department, Instituto Superior Técnico, Technical University of Lisbon.

Sinton, D., 2004. Microscale flow visualization. Microfluid Nanofluid 1, 2–21.

Wereley, S., Gui, L., Meinhart, C., 2002. Advanced algorithms for microscale particle image velocimetry. AIAA J. 40, 1047–1055.

Went, F., 1968. The Size of Man. American Scientist 56, 400–413.

Yu, D., Warrington, R., Barron, R., Ameel, T., 1995. An experimental and theoretical investigation of fluid flow and heat transfer in microtubes. In: Proceedings of ASME/JSME Thermal Engineering Joint Conference, Maui, HI, pp. 523–530.